# *Synthesis of monoclinic and tetragonal chalcocite nanoparticles by iron-induced stabilization.*

Tony Machani, Daniel P. Rossi, Brandon J. Golden, Evan C. Jones, Mona Lotfipour, and Katherine E. Plass*

Department of Chemistry, Franklin & Marshall College, Lancaster, PA 17604

Supporting Information Available.

## I. Experimental:

Sulfur (99.98%), copper(II) acetylacetone (Cu(II)(acac)$_2$, ≥99.99%) and iron(III) acetylacetonate (Fe(III)(acac)$_3$, ≥99.9%) were obtained from Sigma-Aldrich and used as received. cis-1-Amino-9-octadecene (70%), also called oleylamine, was dried over molecular sieves.

*Typical reaction*: Cu(acac)$_2$ (0.52680 g, 2.01 mmol), Fe(III)(acac)$_3$ (0.03591 g, 0.10 mmol), and sulfur (0.03275 g, 1.02 mmol) were added to a 3-neck, 50 mL round bottom flask equipped with a reflux condenser and stir bar. Oleylamine (20 mL) was added and the reaction vessel was purged with argon gas for 20 minutes with stirring before heating commenced. The reaction was held at 200 °C for 1 hour, then 260 °C for 1 hour. The reaction was cooled to room temperature and centrifuged at 6000 rpm for 10 min in a 50 mL centrifuge tube. The precipitate was suspended in THF, precipitated with acetone, and then centrifuged to purify the particles. To ensure removal of reactants, the precipitate was again suspended in THF, precipitated with acetone, and then centrifuged to purify the particles.

*Powder X-ray diffraction (PXRD):* PXRD samples were prepared by casting nanoparticle samples onto glass slides from THF or CH$_2$Cl$_2$. PXRD experiments were carried out using a PANalytical X'Pert Pro X-ray diffractometer using Cu Kα radiation. The accelerating voltage and current were 45 kV and 40 mA, respectively. Scans were collected from 10 to 75 °2θ. 10 repetitions were summed. The samples were then analyzed using the program PANalytical X'Pert HighScore Plus (Version 2.2e), which allowed comparisons with the ICDD powder X-ray diffraction pattern database (PDF Release 2).

*UV/visible/NIR absorption spectroscopy*: Samples were collected using a Perkin-Elmer Lambda 9/19 spectrometer. Absorbance in the range 1600 nm to 400 nm was measured at 480 nm/min. Samples were placed in quartz cuvettes intended for use in the near-infra red through visible wavelength regions.

*Transmission electron microscopy (TEM):* TEM samples were prepared by solvent-casting samples onto Cu-supported TEM grids with carbon coating. The microscope employed was a JEOL JEM-1005X Electron Microscope.

*Energy dispersive X-ray spectroscopy (EDS):* EDS was carried out using a JEOL 7500F scanning electron microscope equipped with an Oxford Inca Thin Window 10$^2$ mm EDS housed in the Penn Regional Nanotechnology Facility. Powder samples were immobilized on conductive carbon tape.

*X-ray photoelectron spectroscopy (XPS):* XPS was carried out using a Scienta ESCA-300 housed at Lehigh University. Particle samples cast on Si wafers were analyzed under high vacuum with monochromatic Al Kα X-rays. A flood gun was used for charge compensation. Wide energy scans from 0 to 1200 eV binding energy were employed to identify elements on the surface, and high resolution spectra were captured for Cu, Fe, and S 2p regions and the Cu and Fe 3p region.

II. Distinguishing djurleite and α-chalcocite by PXRD.

Distinguishing djurleite and α-chalcocite requires careful comparison of the PXRD patterns (Figures S1a,b). The most intense peaks in the PXRD patterns of djurleite and α-chalcocite (around 48, 46, and 38°) are nearly identical, varying at most by 1.3° 2θ, and both are accompanied by many small and overlapping peaks from 25 to 38° 2θ and from 53 to 56° 2θ. The three most intense peaks in the djurleite PXRD pattern are expected to occur at higher 2θ values than those of α-chalcocite (48.6, 46.3, and 37.6° 2θ in djurleite compared to 47.4, 46.0, and 37.4° 2θ in α-chalcocite), according to calculated PXRD patterns. The program Mercury (ver. 2.2, Build RC5, Cambridge Crystallographic Data Center) was used to calculate PXRD patterns using single crystal X-ray structures obtained by Evans[1] for both α-chalcocite (100333-ICSD) and djurleite (100334-ICSD), both available in the Inorganic Crystal Structure Database (FIZ Karlsruhe, 2010). For α-chalcocite sample (Figure 1b), these peaks (48.4, 45.9, and 37.4) are indeed shifted to 2θ values lower than the djurleite sample shown in Figure 1a (48.7, 46.4, and 37.6). Furthermore, the peak shape at 46° 2θ is distinct in the two different phases. α-Chalcocite has shoulder peaks on either side of 46° 2θ, whereas djurleite has two very close peaks which appear as one peak much narrower than that seen for α-chalcocite. Again, this behavior is confirmed in Figures 1a and b. Moreover, examination of calculated and experimental PXRD patterns revealed several additional distinguishing features of djurleite and α-chalcocite amongst the many low-intensity peaks that coincide or overlap. α-Chalcocite is marked by two peaks at 38.60 and 40.75° that are much more intense than peaks in djurleite, and by peaks at 30.20 and 32.80° which are absent in djurleite. While most of the small peaks in the djurleite pattern are coincident with peaks in α-chalcocite, unique peaks at 26.20 and 55.75° allow confirmation of djurleite formation. The experimental powder patterns contained in the International Centre for Diffraction Data database that best matched the calculated patterns, [023-0959] for djurleite and [033-0490] and [023-0961] for α-chalcocite, were used for identification purposes. Pattern [023-0961] is marked as deleted by the ICDD because it duplicates [033-0490] and because the unit cell is given as orthorhombic, an assignment that has since been corrected to monoclinic. The [023-0961] pattern, however, matched the calculated pattern and had more high 2θ data than [033-0490]. For Figures 1a,b, the overlays are the calculated patterns from the ICSD because there were small observed peaks that were not present in the database patterns, but were present in the calculated patterns.

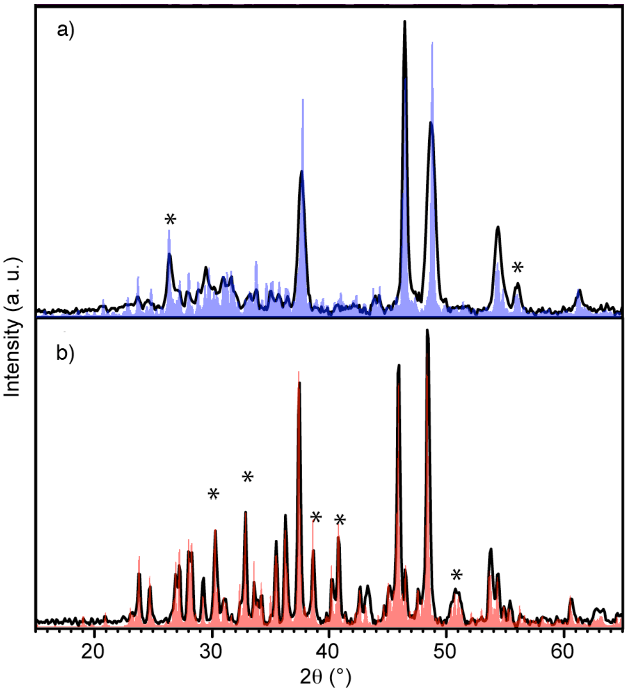

**Figure S1.** a) PXRD pattern of djurleite nanoparticles with the calculated powder pattern from 100334-ICSD overlaid in blue and b) PXRD pattern of α-chalcocite nanoparticles with the calculated powder pattern from 100333-ICSD overlaid in red.

### III. Figure S2. X-ray photoelectron spectroscopy of tetragonal and iron-stabilized monoclinic chalcocite nanoparticles.

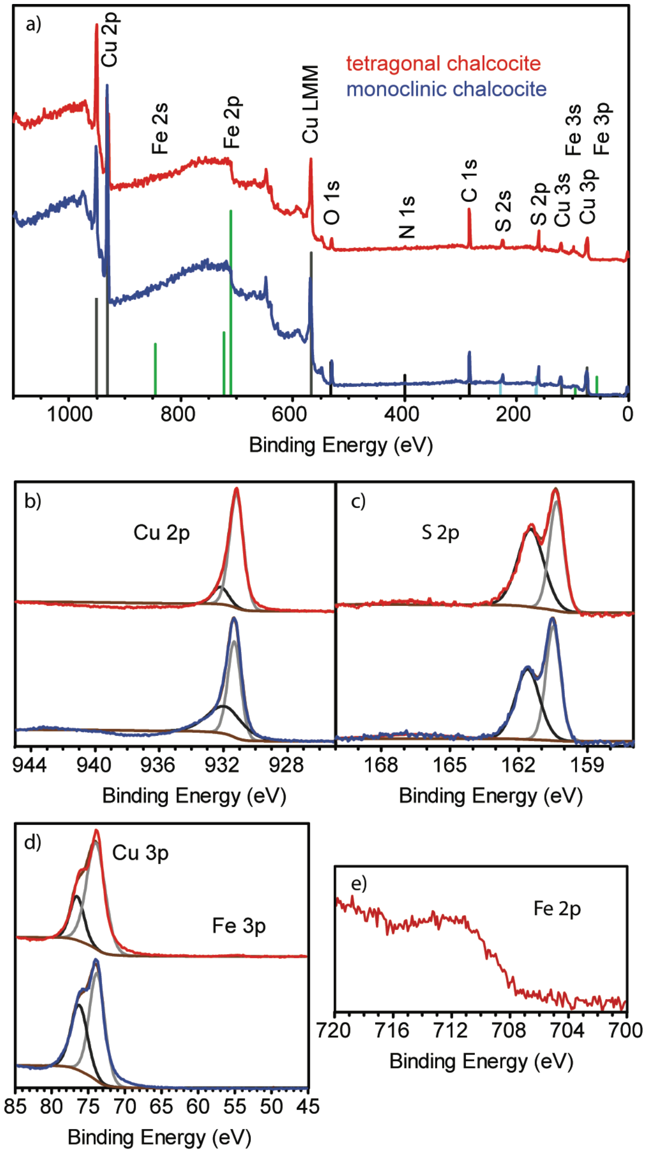

**Figure S2.** X-ray photoelectron spectroscopy data for tetragonal (red) and Fe-stabilized monoclinic chalcocite (blue) nanoparticles. a) Survey scans show the presence of Cu, S, C, and O in both species, while Fe is observable only in the tetragonal chalcocite particles. b) The Cu 2p regions show that Cu is present primarily in the +1 oxidation state in both particles, with a peak around 931.5 eV.[2] A shoulder peak around 932 eV suggests some $Cu^{2+}$ is present. c) The S 2p regions exhibit both peaks expected due to 2p(1/2) and 2p(3/2). The broadness of the peaks, however, suggests that S ions at the surface are not in uniform environments. d) The Cu and Fe 3p region allows comparison of the amount of Fe present at the surface of these particles. While tetragonal particles exhibit a peak for Fe 3p that is barely above the baseline (0.6% of total Cu 2p + Fe 2p area), no Fe peak can be observed for the monoclinic particles. e) The Fe 2p region of the tetragonal particles shows a broad peak from 708 to 716 binding eV. This region is consistent with $Fe^{2+}$ found in FeS (713.60 to 710.30 eV) and $FeSO_4$ (713.60 eV).[3] Several iron oxide species ($Fe_3O_4$ and $Fe_2O_3$) have spectral lines peaks from 711.60 eV to 708.10 eV.[3]

(1) Evans, H. T. *Nat.-Phys. Sci.* **1971**, *232*, 69-&.

(2) Platzman, I.; Brener, R.; Haick, H.; Tannenbaum, R. *J. Phys. Chem. C* **2008**, *112*, 1101-1108.

(3) Wagner, C. D.; Naumkin, A. V.; Kraut-Vass, A.; Allison, J. W.; Powell, C. J.; Rumble, J. R. *NIST Standard Reference Database 20, Version* 3.5, 2003.

IV. Figure S3. PXRD patterns of monoclinic chalcocite particles monitored over time stored under ambient conditions.

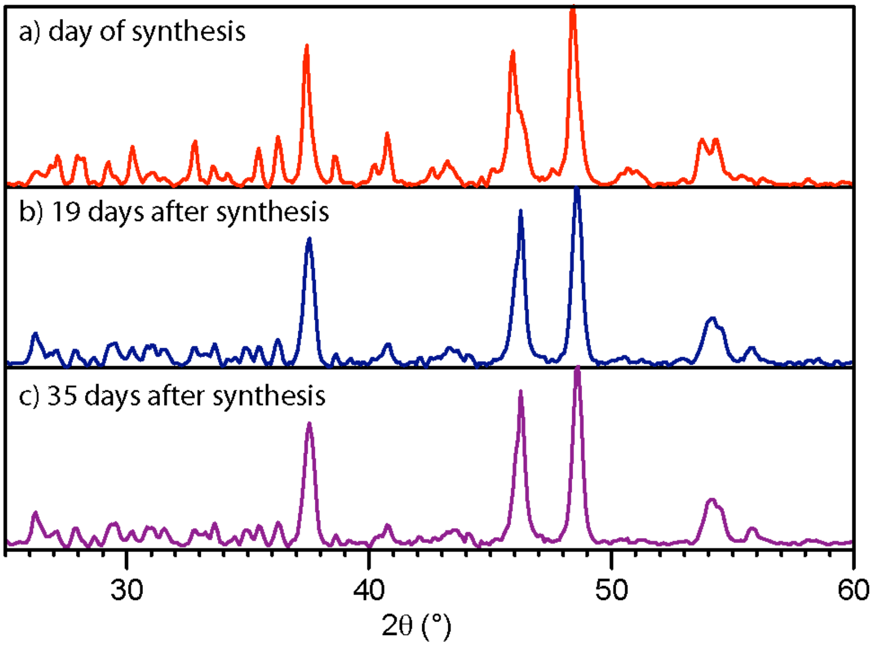

Figure S3. PXRD patterns of monoclinic chalcocite particles monitored over time stored under ambient conditions. Peaks due to monoclinic chalcocite are still apparent after 35 days, whereas similar materials synthesized with the same Cu:S ration but without addition of iron to the reaction mixture convert completely to djurleite in less than a week.

V. Figures S4, S5, and S6. The diffraction peaks observed in the PXRD pattern of obtained particles are compared to the database PXRD patterns for tetragonal chalcocite and common copper sulfide phases (Figure S4), copper iron sulfide phases (Figure S5), and iron sulfide phases (Figure S6).

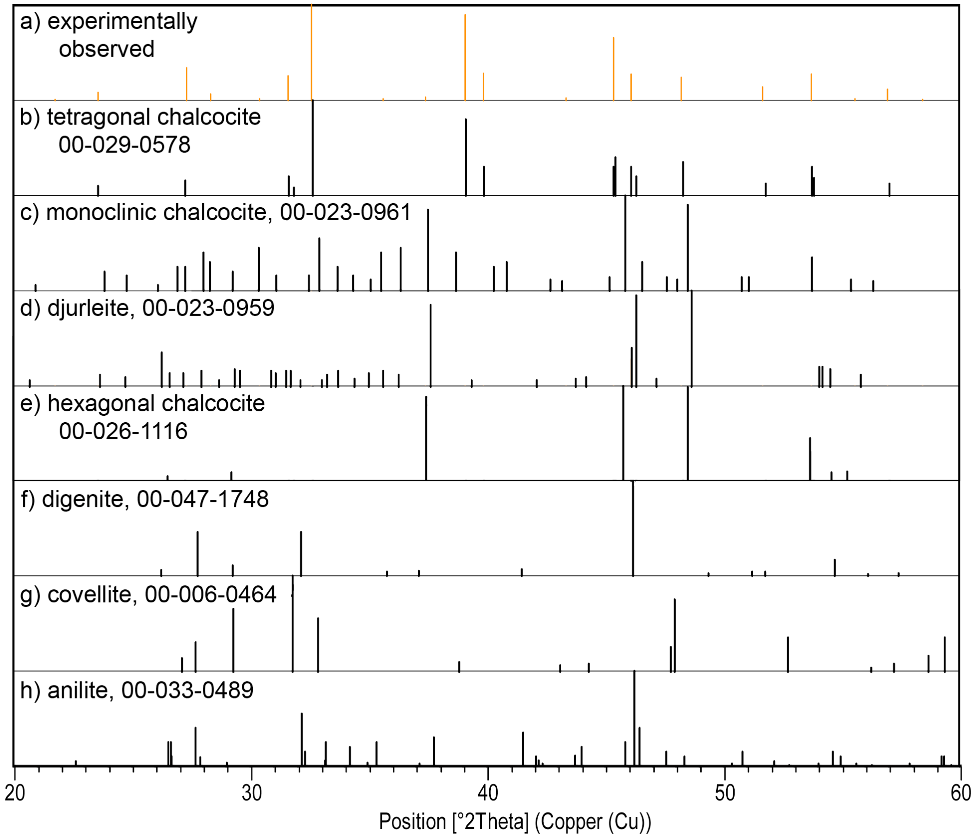

Figure S4. The peaks observed in the PXRD pattern of particles obtained from 2.0 mmol Cu(II)(acac)$_2$, 1.0 mmol S, and 0.1 mmol Fe(III)(acac)$_3$ in 20 mL oleylamine (a) are compared to the database PXRD patterns for tetragonal chalcocite (b) and common copper sulfide phases. Shown are (c) monoclinic chalcocite, (d) djurleite ($Cu_{1.97}S$), (e) hexagonal chalcocite, (f) digenite ($Cu_{1.80}S$), (g) covellite (CuS), and (h) anilite ($Cu_{1.75}S$). The ICDD database reference numbers are given.

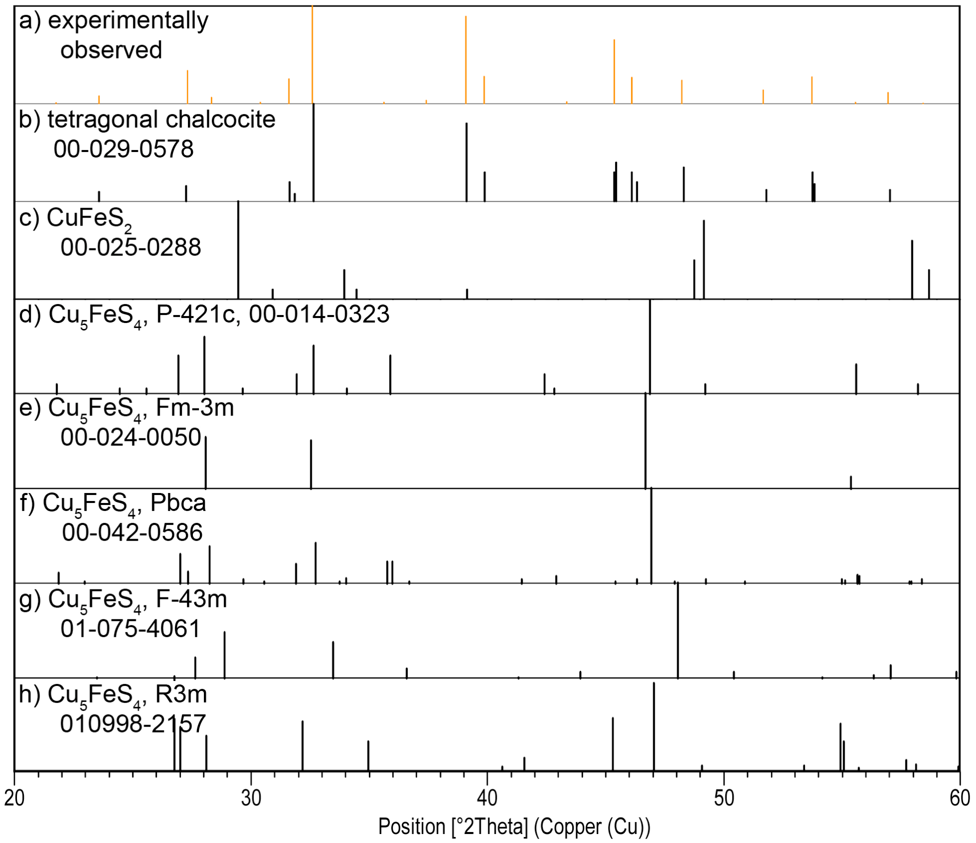

Figure S5. The peaks observed in the PXRD pattern of particles obtained from 2.0 mmol Cu(II)(acac)$_2$, 1.0 mmol S, and 0.1 mmol Fe(III)(acac)$_3$ in 20 mL oleylamine (a) are compared to the database PXRD patterns for tetragonal chalcocite (b) and copper iron sulfide phases. Shown are (c) chalcopyrite ($CuFeS_2$) and (d-h) variations of bornite ($Cu_5FeS_4$). The ICDD database reference numbers are given.

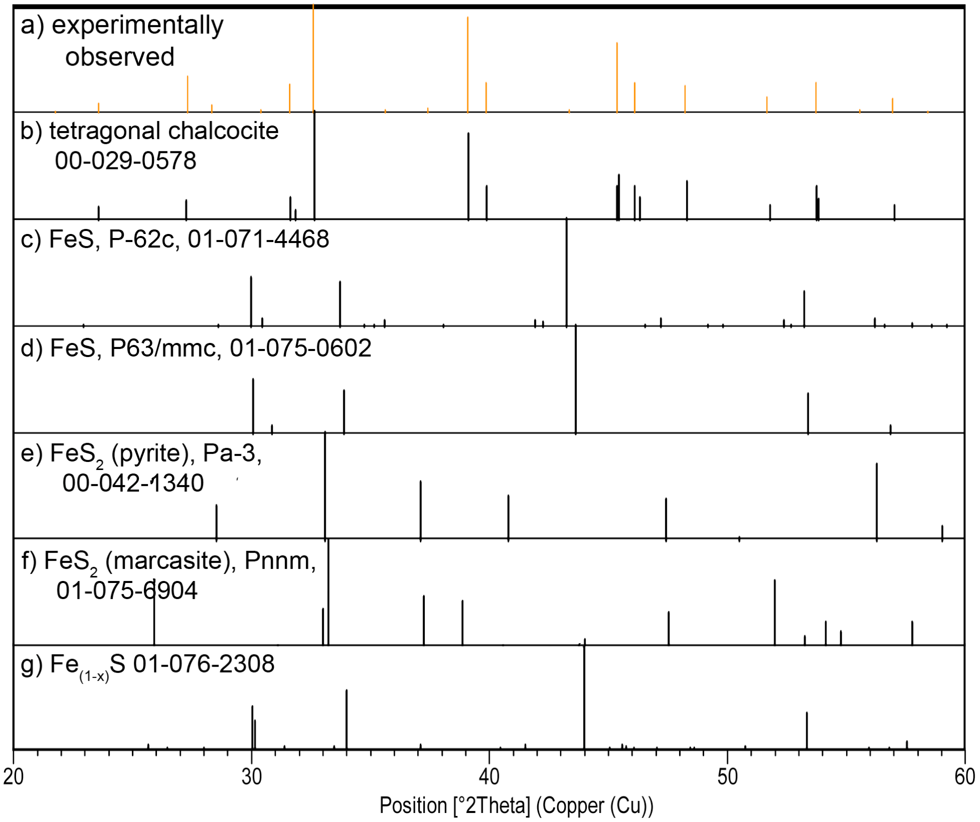

Figure S6. The peaks observed in the PXRD pattern of particles obtained from 2.0 mmol Cu(II)(acac)$_2$, 1.0 mmol S, and 0.1 mmol Fe(III)(acac)$_3$ in 20 mL oleylamine (a) are compared to the database PXRD patterns for tetragonal chalcocite (b) and common copper sulfide phases. Shown are (c-d) two forms of troilite (FeS), (e) pyrite (FeS$_2$), (f) marcasite (FeS$_2$), and (g) pyrrhotite (Fe$_{1-x}$S). The ICDD database reference numbers are given.

VI. Figure S8. PXRD patterns of tetragonal chalcocite particles monitored over time stored under ambient conditions.

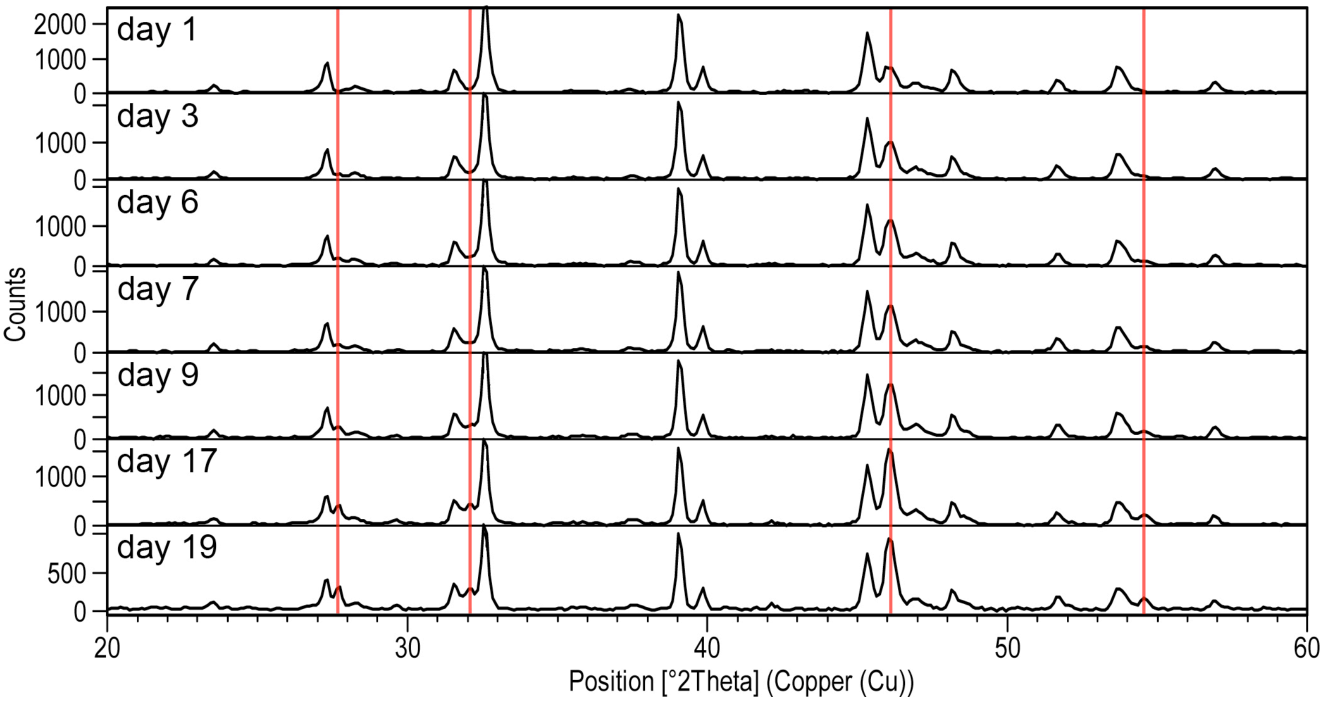

Figure S8. PXRD patterns of tetragonal chalcocite particles monitored over time stored under ambient conditions. Prominent peaks indicative of rhombohedral digenite are marked in red, and clearly grow over time, starting on day 6, though they are still lower in intensity than the tetragonal chalcocite peaks.

VII. Table S1 and Figure S9. Comparison of the unit cell parameters for cubic, tetragonal, and orthorhombic forms of iron, chromium, and cobalt sulfides to those of tetragonal chalcocite.

Table S1. Unit cell parameters for cubic, tetragonal, and orthorhombic forms of iron, chromium, and cobalt sulfides as well as those of tetragonal chalcocite. The space group and Inorganic Crystal Structure Database (ICSD) structure number are also included.

| | a (Å) | b (Å) | c (Å) | Space group | Crystal class | ICSD identifier |
|---|---|---|---|---|---|---|
| $FeS_2$ (marcasite) | 3.387 | 4.443 | 5.425 | Pnn2 | orthorhombic | 42415-ICSD |
| $Cr_3S_4$* | 3.4216 | 5.9534 | 11.249 | C 2/m | monoclinic | 81886-ICSD |
| **FeS (mackinawite)** | **3.674** | **3.674** | **5.033** | **P4/nmm** | **tetragonal** | **81087-ICSD** |
| **tetragonal chalcocite** | **3.996** | **3.996** | **11.287** | **$P4_32_12$** | **tetragonal** | **16550-ICSD** |
| MnS (NaCl) | 5.24 | 5.24 | 5.24 | $Fm\bar{3}m$ | cubic | 18007-ICSD |
| $CuFeS_2$ | 5.2289 | 5.289 | 10.423 | $I\bar{4}2d$ | orthorhombic | 2518-ICSD |
| $FeS_2$ (pyrite) | 5.416 | 5.416 | 5.416 | $Pa\bar{3}$ | cubic | 109377-ICSD |
| $CoS_2$ (pyrite) | 5.539 | 5.539 | 5.539 | $Pa\bar{3}$ | cubic | 86351-ICSD |
| $Cu_5FeS_4$ (high polymorph) | 5.47 | 5.47 | 5.47 | F23 | cubic | 24174-ICSD |
| MnS (zinc blende) | 5.59 | 5.59 | 5.59 | $F\bar{4}3m$ | cubic | 76205-ICSD |
| $MnS_2$ (pyrite) | 6.104 | 6.104 | 6.104 | $Pa\bar{3}$ | cubic | 36549-ICSD |
| $Co_3S$ ($Al_2MgO_4$) | 9.405 | 9.406 | 9.406 | Fd3m | cubic | 24212-ICSD |
| $Co_9S_8$ | 9.928 | 9.928 | 9.928 | $Fm\bar{3}m$ | cubic | 23929-ICSD |

*$Cr_3S_4$ was included despite belonging to the monoclinic crystal class because it is nearly tetragonal with $\gamma = 91.5°$.

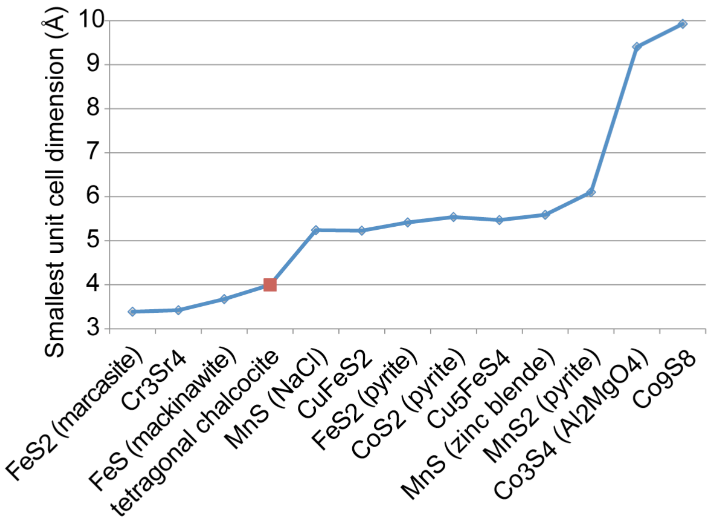

Figure S9. The smallest unit cell parameter for cubic, tetragonal, and orthorhombic forms of iron, chromium, and cobalt sulfides compared to those of tetragonal chalcocite (red). Tetragonal chalcocite has a smallest dimension most similar to mackinawite (FeS).